Yu Dong, Thomas Bickford, Hazim J. Haroosh, Kin-Tak Lau, Hitoshi Takagi, Appl. Phys. A (2013) 112: 747-757.

Multi-response analysis in the material characterisation of electrospun poly (lactic acid)/ halloysite nanotube composite fibres based on Taguchi design of experiments: fibre diameter, non-intercalation and nucleation effects

Yu Dong [a,*], Thomas Bickford [a], Hazim J. Haroosh [b], Kin-Tak Lau[c], Hitoshi Takagi[d]

[a] *Department of Mechanical Engineering, Curtin University of Technology, Perth WA 6845, Australia*
[b] *Department of Chemical Engineering, Curtin University of Technology, Perth WA 6845, Australia*
[c] *Department of Mechanical Engineering, The Hong Kong Polytechnic University, Hung Hom, Kowloon, Hong Kong, China*
[d] *Advanced Materials Division, Institute of Technology and Science, The University of Tokushima, Tokushima 770-8506, Japan*

Abstract

Poly (lactic acid) (PLA)/halloysite nanotubes (HNT) composite fibres were prepared by using a simple and versatile electrospinning technique. The systematic approach via Taguchi design of experiments (DoE) was implemented to investigate factorial effects of applied voltage, feed rate of solution, collector distance and HNT concentration on the fibre diameter, HNT non-intercalation and nucleation effects. The HNT intercalation level, composite fibre morphology, their associated fibre diameter and thermal properties were evaluated by means of X-ray diffraction (XRD) analysis, scanning electron microscopy (SEM), imaging analysis and differential scanning calorimetry (DSC), respectively. HNT non-intercalation phenomenon appears to be manifested as reflected by the minimal shift of XRD peaks for all electrospun PLA/HNT composite fibres. The smaller-fibre-diameter characteristic was found to be sequentially associated with the feed rate of solution, collector distance and applied voltage. The glass transition temperature (T_g) and melting temperature (T_m) are not highly affected by varying the material and electrospinning parameters. However, as the indicator of the nucleation effect, the crystallisation temperature (T_c) of PLA/HNT composite fibres is predominantly impacted by HNT concentration and applied voltage. It is evident that HNT's

* Corresponding author. Tel.: +61 8 92669055; fax: +61 8 92662681.
E-mail address: Y.Dong@curtin.edu.au (Y. Dong).

nucleating agent role is confirmed when embedded with HNTs to accelerate the cold crystallisation of composite fibres. Taguchi DoE method has been found to be an effective approach to statistically optimise critical parameters used in electrospinning in order to effectively tailor the resulting physical features and thermal properties of PLA/HNT composite fibres.

Keywords: halloysite nanotube; polymer composite; electrospinning; Taguchi design of experiments; material characterisation

1. Introduction

Electrospinning is a continuous fibre-production technique which has been developed almost a century ago with its first apparatus patented in 1934 [1, 2]. The fundamental principle of electrospinning lies in the formation of uniform nanofibres by means of the ejection of a polymer solution in a high-voltage electrical field. Accordingly, electrostatic repulsive force is applied to overcome the surface tension and thus elongate the jet solution into fibrous structures in the perpendicular direction to the material collector.

In recent years, the popularity of electrospinning used in nanotechnology areas has been evidenced for the cost-effective production of continuous nanofibres owing to its enormous innovative applications [3]. These implementations can range from tissue engineering for skin grafts [4, 5], construction and building structures such as fibre reinforcement of structural materials [6], drug delivery with better release control [7-9], cosmetic membranes [10], nanofiltration of gasses and liquids [11, 12] to military protective clothing [10]. The size effect of electrospun fibres is of particular concern in that the significant reduction of fibre diameter down to the nanoscaled level enables to produce fibre networks with large fibre aspect ratio, high specific area and porosity. These structural merits are very crucial for the enhancement of mechanical properties of fibrous structures, the cell growth in tissue scaffolds based on electrospun fibre mats, and the acceleration of drug release.

Halloysite nanotubes (HNTs) has the chemical structure with a composition of $Al_2Si_2O_5(OH)_4 \cdot nH_2O$, which belongs to a kaolin family as a unique inorganic filler.

Relatively cheap HNTs resemble the similar structure of carbon nanotubes (CNTs) in geometry with a longitudinal hollow structure by rolling the layers of tetrahedral sheets of silica and octahedral sheets of alumina [13, 14]. HNTs obtained from diverse sources differ in size, and the normal dimension of HNTs can be 300-1500 nm in length, 15-100 nm for the inner diameter and 40-120 nm for the outer diameter [15]. There is a wide range of applications using HNTs such as filler reinforcements, cosmetics, catalyst carriers, ceramics and drug delivery due to their unusual shape and geometry, surface property, chemical formation and cost-effectiveness [16]. In particular, HNTs have been shown to be a promising drug carrier, which can develop novel drug delivery systems via electrospinning with sustained release property for the medical applications in pharmaceutical area and tissue scaffolding [17, 18].

However, current challenges encountered to electrospun nanofibres comprise the non-uniformity of fibre diameter for their fineness and dimensional stability, and critical defects such as beads and internal pores observed on produced fibres. These problems can be tackled effectively by a good control of material and processing parameters including solution viscosity, feed rate and electrical conductivity, applied voltage and collector distance, etc. For instance, increasing the viscosity of poly (ethylene oxide) (PEO) solution was found to reduce the formation of beads [10] while smoother PEO nanofibres were produced when decreasing the applied voltage [19]. Furthermore, the additional filler material into a polymer solution has also been shown to contribute to the free-of-bead fibres, as evidenced by electrospinning biodegradable Poly-D-lactide (PDLA) polymer with 1 wt% salt addition [20].

The present research has not yet holistically investigated the optimisation of electrospinning process in a systematic manner, which is conventionally limited to the determination of physical, thermal and structural properties of electrospun nanofibres/nanocomposites with the fixed processing and material parameters [21-23]. As a result, the tailored fibre structures and properties, as well as the fibre quality control may potentially diminish leading to the narrow-down of application scopes. To overcome such

manufacturing drawback, this paper presents a robust statistical Taguchi design of experiments (DOE) to evaluate systematically the effects of applied voltage, feed rate of solution, collector distance and HNT concentration on the fibre diameter, HNT non-intercalation and nucleation in PLA/HNT composite fibres. The optimum processing conditions were determined to improve the material performance and yield higher productivity of electrospun composite fibres with good quality.

2. Experimental details

2.1. Materials and fabrication procedure

Natureworks ® PLA (Grade 6202D) biopolymer pellets (relative viscosity: 3:1 and melt flow index at 210ºC: 15-30 g/10 min) were supplied by Jamplast Inc. (Ellisville, MO USA). These pellets are generally used for extrusion into mechanically drawn staple fibres using conventional fibre spinning or drawing equipment. Chloroform and acetone with 99.9% purity at a constant volume ratio of 2:1 are used in this study as co-solvents. The premium ultrafine HNTs are typical hydrated aluminium silicates which were donated by Imerys Tableware Asia Limited, New Zealand. About 1wt% BYK 9076 dispersant (Byk-Chemie, Melbourne, Australia) was added to prepare mixture solutions to alleviate the problem of HNT sedimentation encountered in the electrospinning process.

12 g PLA pellets were dissolved in 100 ml chloroform/acetone co-solvents to produce a fixed 12 wt% PLA solution as recommended in our previous work [21]. The mixing step took 4 h with the aid of an orbital shaker incubator (model TU-400, Thermoline Scientific Pty. Ltd, Australia) at 150-200 rpm and 55ºC. Subsequently, 30 g HNT powders were added to the same 100 ml co-solvents, further subjected to the ultrasonication process for 3-4 h by using an ultrasonic cleaning unit ELMA® Ti-H-5. Such prepared HNT solution was magnetically stirred for about 9 h at 750 rpm and 125 ºC until co-solvents were fully removed. Sonicated HNT powders were then mixed with prepared PLA solution to produce three different HNT concentrations of 1.5, 5, 10 wt%. In this step, BYK9076 dispersant was

transferred into PLA-HNT solution using an ultrasensitive pipette. The final solution was again mixed by the orbital shaker incubator for 1 h to achieve an adequate HNT dispersion.

In the electrospinnig process, different prepared solutions were placed into a 10 ml plastic syringe with a 21 gauge hypodermic metal needle. The feed rate of solution and applied voltage were controlled by a Fusion 100 syringe pump (Chemyx Inc. Stafford, TX USA) as well as an ES30P-5 W high voltage power supply (Gamma High Voltage Research, Ormond Beach, FL USA), respectively. A mesh collector covered by aluminium foils stood vertically with the manual adjustment of needle tip-to-collector distance to obtain different batches of electrospun fibre mats. The entire electrospinning apparatus was located in a transparent acrylic housing case inside a fume cupboard for the slow solvent removal. The processing parameters used in this study are detailed in the following Taguchi DoE layout.

2.2. Taguchi experimental design

The design of experiments (DoE) is a very robust experimental design technique that can explore the significant factorial effects and optimum conditions in modern manufacturing industries. A large complex number of factors are often involved for the systematic DoE analysis so that the non-significant variables can be eliminated at the earlier stage. Based on the recent work on the DoE evaluation of manufacturing polymer nanocomposites [24, 25], a L_9 DoE orthogonal array was selected with four factors of applied voltage, collector distance, feed rate of solution and HNT concentration at three different levels (level 1: “low” setting, level 2: “intermediate” setting and level 3; “high” setting), which makes up 9-trial runs as illustrated in Tables 1 and 2. For simplicity, it is hypothesised that the factorial interactions are neglected in this DoE analysis, which is a typical design criterion in the L_9 array. In comparison to the conventional full factorial experimental design with 81 (3^4) runs, the advantage of Taguchi L_9 DoE array can be attributed to the significantly reduced number of trials while the analysed results are still kept at a satisfactory level to save experimental time and associated cost.

The experimental observations are further transformed into signal-to-noise (S/N) ratio and a typical performance characteristic is involved as follows:

Smaller-the-better characteristic: $$S/N = -10\ log\left(\frac{1}{n}\sum_{i=1}^{n} y_i^2\right) \quad (1)$$

where n is the number of observations in each run, and y is the measured response data. The responses in this DoE analysis consist of average fibre diameter d_{aver} from 20 fibre observations per run and cold crystallisation temperature (T_c) of PLA/HNT composite fibres due to the HNT nucleation effect [21].

For the process optimisation, a simplified Pareto analysis of variance (ANOVA) is employed, which does not require the ANOVA table and F-tests [26]. The significant factors and optimum conditions are detected based on the derived cumulative contribution percentage of about 85% in this study while economical and technical issued are taken into account for other non-significant factors.

2.3. Material characterisation

A Philips XL30 field emission scanning electron microscope was operated at an accelerating voltage of 15 kV with the working distance at 4.5-5.5 mm for examining morphological structures of electrospun composite fibre mats. Prior to this, these mats were sputter coated with platinum. The associated SEM micrographs were analysed using ImageJ® software developed by National Institutes of Health (NIH), USA. Twenty fibres per image and three different positions on each fibre were chosen as the measurement criterion to determine the average fibre diameter.

The HNT intercalation level was investigated by a wide angle X-ray diffraction (WAXD) with Bruker D8 ADVANCE diffractometer (Germany) to see the change of HNT d-spacing when HNTs were embedded into the PLA matrix. The Cu-K_α source (wave length λ =0.1541 nm) was operated at 40 kV and 40 mA. The XRD samples consisting of as-received HNT powders and composite fibre mats were scanned from 2θ = 5-40º at the scan rate of 0.013°/s.

The thermal properties of as-received PLA pellets and electrospun composite fibre mats were evaluated via a PerkinElmer DSC6000 (Waltham, Massachusetts, USA) based on differential scanning calorimetry (DSC). About 5-10 mg DSC samples were heated from 30 to 200ºC at the heating rate of 10ºC/min and then remained in an isothermal condition at 200ºC for 5 min. At the cooling step, these samples were cooled down to 30 ºC at the cooling rat of 20ºC/min. The same heating/cooling cycles were repeated for a second run. The glass transition temperature (T_g), cold crystallisation temperature (T_c) and melting temperature (T_m) were assessed from the second heating cycles. DSC tests were repeated and three measurements per DoE trial run were made to ensure the good reproducibility of the results. As-received PLA pellets were also examined twice in the identical condition as the material benchmark for thermal properties.

3. Results and discussion

3.1. Surface morphology and distribution of fibre diameter

SEM micrographs of composite fibre morphology in DoE study and corresponding determined average fibre diameters are illustrated in Fig. 1 and Table 3. On a global scale, random fibre distribution is evident in most mat samples due to using a stand-alone mesh collector with little fibre alignment control. However, some large fibres with the diameter over 1μm appear to be locally aligned in either almost vertical (ES#2 and ES#6) or diagonally oriented (ES#5 and ES#6) directions. Prevalent non-uniform fibre structures are detected mainly in ES#2, ES#5 and ES#8 with the diameter variation from 200 nm to 3μm. In addition, large entangled fibre aggregates are shown in ES# 3 and ES#7, resulting from the hindrance of fibrous structures from the solution jet. This typical phenomenon can be due to the combined effect of higher feed rate at 4 ml/h and excessive amount of undispersed HNT taking place at higher HNT concentrations of over 5 wt% [21]. When more solution droplets were ejected from the needle tip per hour, these droplets with excessive HNTs did not have sufficient time to be elongated to individual fibres with relatively small fibre sizes, which were then directly received from the mesh collector. As a result, fibre aggregates or bundles

become more evident due to the lack of fibre stretching/elongation. The other small-bead defects are noticed in ES#4, ES#6 and ES#8, which may arise from the clogging problem of high-concentration HNT encountered at the needle tip. As a result, droplets were formed with the flow instability to deteriorate the elongated fibrous structures. On the contrary, the fibrous structures become bead-free at the low HNT concentration of 1.5 wt%, as evidenced in ES#1, ES#5 and ES#9 (Figs 1(a), (e) and (i)). Based on summarised average fibre diameter data (d_{aver} ≤1μm) in Table 3, one can get the minimum diameter of 498 nm found in ES#1, followed by ES#4, ES#5, ES#6 and ES#8 in the diameter range of 800-900 nm. The rest of samples have relatively large average fibre diameters of 1.2-1.5μm.

More explicitly, frequency contribution (FR) plots in terms of fibre diameter range in DoE study are demonstrated in Fig. 2. The number of nanofibres expressed by the percentage of frequency contribution (FC) was quantified on the basis of three designated criteria including $d_{aver} \leq$ 1μm, $d_{aver} \leq$ 600 nm and $d_{aver} \leq$ 400 nm, respectively, Table 3. ES#1, ES#4, ES#5, ES#6 and ES#8 possess the frequency contribution in range of 65-90% under the category of $d_{aver} \leq$ 1μm. ES#4 and ES#5 have the similar frequency contributions amongst all the three criteria in good accordance with their close d_{aver}. In comparison, mixed results were observed in ES#2, ES#3, ES#7 and ES#9, where relatively large microsized d_{aver} were determined accordingly, with the frequency contributions of 75, 55, 80 and 80%, respectively for $d_{aver} >$1μm. Besides, ES#9 shows the worst scenario with only 20% frequency contribution for $d_{aver} \leq$ 1μm, indicating the highest level of fibre non-uniformity in this DoE study.

3.2. HNT non-intercalation effect

XRD patterns of as-received HNT powders, electrospun PLA/HNT composite fibres (i.e. ES#1-ES#9) are depicted in Fig. 3, along with their calculated basal spacing d values listed in Table 4, which are based on Bragg's law ($n\lambda=2d\sin\theta$ where n is an integer and θ is the diffraction angle). Three distinct XRD peaks at 2θ =12.09, 19.90 and 24.85° in relation to reflection planes (001), (020), (110) and (002) are observed, which correspond to d=0.732, 0.446 and 0.358 nm, respectively. The missing of 10Å peak (2θ =8.76°) further confirms that

such HNTs are fully dehydrated and thus known as 7Å-halloysite [21, 27]. The (001), (020), (110) and (002) peaks of electrospun composite fibres have been found to be either broadened with much lower peak intensities compared to those of HNTs or completely disappear. This phenomenon suggests that break-down of large HNT agglomerates into finer tubular particles may be achieved in the initial sonication process. The complete disappearance of (020), (110) and (002) peaks mainly take place in ES#1, ES#5 and ES#9 owing to using a low HNT concentration of only 1.5 wt% in those material formulations of DoE study. However, there is no evident change in all relevant XRD peak positions of composite fibres, as opposed to those of as-received HNTs, regardless of variations of material and processing parameters in electrospinning process proposed in Table 2. The corresponding basal spacing *d* values are in range of 0.722-0.732 nm for (001) peaks, 0.442-0.446 nm for (020), (110) peaks, as well as 0.357-0.360 nm for (002) peaks. This finding can be attributed to the non-intercalation effect with limited enlarged interlayers of HNTs. Due to the fundamental electrospinning principle to fabricate continuous nanofibrous structures, the elongation of PLA molecules make it difficult to penetrate into the HNT interlayers. As a matter of fact, these polymeric molecules may be easily embedded onto the outer surfaces of HNTs with good interfacial bonding [21] rather than form the intercalated structures within HNTs. The other plausible explanation can lie in relatively small basal spacing of dehydrated halloysite as opposed to hydrated counterpart, resulting in a tight binding between halloysite platelets to prevent the intercalation of polymeric molecules [27]. Overall, it is manifested that electrospinning process has not played a very significant role in the HNT finer dispersion, especially in term of the intercalation effect.

3.3. DSC thermal analysis

The DSC thermograms for as-received PLA pellets and PLA/HNT composite fibres (ES#1-ES#9) are demonstrated in Fig. 4 and associated thermal parameters of T_g, T_c and T_m are also listed in Table 5. It can be seen clearly that variations of HNT concentrations and processing parameters of electrospinning used in DoE study have a minor impact on both T_g

(in range of 57-62°C) and T_m (in range of 159-162°C for T_{m1} and 166-168°C for T_{m2}) values of PLA. This finding is in good accordance with the previous literatures on prepared PLA/HNT nanocomposites via melt-extrusion [28, 29]. Similar results are also presented for PLA based composites reinforced with popular nanofillers of organo-montmorillonite (OMMT) [30]. Multiple melting peaks in the presence of shoulder-like DSC curve portions have been observed for most material batches except as-received neat PLA, ES#1 and ES#5. This can result from the reason that imperfect PLA crystals, initially melted at a lower temperature, can recrystallise to generate new crystals at a higher temperature [30]. On the other hand, electrospun fibre composite fibres with the addition of HNTs undergo significant shift to lower temperature region for the peak temperature (T_c) of cold crystallisation, which is in range of 106-114°C as compared to 140°C for as-received PLA. In particular, it also appears that ES#4 and ES#8 have much lower T_c values at a high HNT concentration of 10 wt%. This finding coincides well with the previous result [29] that increasing the HNT concentration may further decrease the T_c irrespective of HNT modification. HNTs in a tubular shape have large surface areas and can act as effective nucleating sites to facilitate the PLA crystallisation process, thus resulting in the decreased T_c by embedding HNTs. HNTs evidently resemble other typical nanofillers like carbon nanotubes (CNTs) [31] and MMT [30, 32] for their effective nucleating role in electrospun polymer composite fibres. Since the nucleation effect of HNTs is more significant as characterised by the great variations of thermal parameter T_c, the following DoE study will solely focus on the thermal response to minimise the T_c while ignoring those caused by relatively small changes of T_g and T_m.

3.4. Factorial significance in response to fibre diameter and nucleation effect

As depicted in Fig. 5, the Pareto ANOVA diagrams demonstrate that the effects of processing parameters on two major response including fibre diameter and crystallisation temperature (T_c) were ranked by the contribution percentages of selected L_9 DoE factors. To minimise the fibre diameter, feed rate (factor C) and collector distance (factor B) and applied voltage (factor A) were detected as three significant factors with their contribution

percentages of 34.2, 32.3 and 19.1%, respectively, Fig. 4(a). The concurrent control of these factors can ensure the fabrication of proper small-diameter fibrous structures with sufficient elongation and bending instability [33, 34]. Besides, the resulting electrostatic force becomes great enough to overcome the surface tension of electrospun solution droplets. HNT concentration as factor D only shows very trivial effect with the lower contribution percentage of only 14.4%. This finding may imply that the viscosity of final prepared solution can be affected more remarkably by the PLA concentration (currently fixed at 12 wt% in this study) as compared to HNT concentration. On the other hand, HNT concentration (factor D)-50.4% and applied voltage (factor A)-44.2% in contribution percentages were determined as the first and second most prevalent factors for minimising the T_c values; whereas, collector distance (factor B)-2.74% and feed rate (factor C)-2.69% appear to be insignificant. Overall, the existence of HNT within PLA matrices is essential for the acceleration of PLA cold crystallisation process, which may further facilitate the enhanced mechanical properties of composite fibres.

3.5. Statistically determined optimum conditions in ANOVA results

The sum of S/N ratio was employed in ANOVA analysis to determine the best level combination in the individual optimum conditions, as shown in Fig. 6. It is based on the criterion that mathematically higher sum of *S/N* ratio can lead to the better performance for effects of significant factors. Certainly the technical and economical issues should also be taken into account for the overall cost-effectiveness between processing and performance in the actual experimental design. The finally determined factorial level combinations in response to fibre diameter and T_c are also summarised in Figs. 6(a) and (b), respectively, in terms of detailed optimum processing conditions and estimates of error variance. The best combination of significant factors to get small fibre diameter is at level 1 for both feed rate and collector distance, and at level 2 for applied voltage, resulting in $A_2B_1C_1D_1$ for all factors. To achieve low T_c, it is suggested that level 3 of HNT concentration and level 2 of applied voltage provide the best combination of $A_2B_3C_1D_3$ along with the level 3 of collector distance

and level 1 of feed rate for two non-significant factors. Though generally sub-optimisation of factorial level can be achieved for the individual response, it is often not realistic to obtain all the expected responses simultaneously with the same optimum combination of factors. Sometimes, a "trade-off" for the overall optimum conditions can take place for the entirely global design of experiments [24, 35].

4. Conclusions

PLA/HNT composite fibres were electrospun according to the four-factor and three-level L_9 Taguchi design of experiments in order to evaluate the effect of material and processing parameters on the composite fibre diameter, and HNT intercalation level and nucleation effect. Electrospinning process has been shown not to facilitate the HNT dispersion in terms of the intercalated structures as evidenced by the little change of XRD peaks regardless of the varied DoE factors. Such non-intercalation phenomenon may suggest that certain pre-treatment of HNTs at the early stage of solution preparation is necessary to improve more uniform HNT dispersion since electrospinning is mainly used to produce elongated polymeric fibrous structures. Furthermore, the influence of different DoE factors and levels on T_g and T_m also appears to be insignificant with only minor alterations of these two critical thermal parameters. The reduction of fibre diameter has been found to be due to the control of three sequentially significant factors feed rate, collector distance and applied voltage. The nucleating effect resulting from embedded HNT was manifested owing to the most significant factor of HNT concentration to induce the lower T_c for more rapid PLA cold crystallisation process, which is followed by applied voltage as the second significant factor. The combination of Taguchi DoE and Pareto ANOVA becomes an effective statistical approach to mathematically determine individual optimum conditions for the fabrication of electrospun PLA/HNT composite fibres.

Acknowledgements

Authors wish to acknowledge the financial support from Curtin Internal Research Grants (IRG) 2010 (project No.: 47604) to undertake this work. The authors are also indebted to Ms.

Elaine Millers and Dr. Cat Kealley from Centre for Materials Research at Curtin University for technical assistance with SEM and XRD, respectively.

References

[1] Y. A. Dzenis, Science **304**, 1917 (2004)

[2] D. H. Reneker, I. Chun, Nanotechnology **7**, 216 (1996)

[3] W.E. Teo, S. Ramakrishna, Compos. Sci. Technol. **69**, 1804 (2009)

[4] Y. Zhou, D. Yang, X. Chen, Q. Xu, F. Lu, J. Nie, Biomacromolecules **9**, 349 (2008)

[5] H. M. Powell, S. T. Boyce, Tissue Eng.: Part A **15**, 2177 (2009)

[6] M. M. Bergshoef, G. J. Vancso, Adv. Mater. **11**, 1362 (1999).

[7] E. Luong-Van, L. Grøndahl, K. N. Chua, K. W. Leong, V. Nurcombe, S. M. Cool, Biomaterials **27**, 2042 (2006).

[8] J. Zeng, X. Xu, X. Chen, Q. Liang, X. Bian, L. Yang, X. Jing, J. Control. Release **92**, 227 (2003)

[9] D. G. Yu, X. X. Shen, C. Branford-White, K. White, L. M. Zhu, S. W. A. Bligh, Nanotechnology **20**, 055104 (2009)

[10] Z. M. Huang, Y. Z. Zhang, M. Kotaki, S. Ramakrishna, Compos. Sci. Technol. **63**, 2223 (2003)

[11] Y. C. Ahn, S. K. Park, G. T. Kim, Y. J. Hwang, C. G. Lee, H. S. Shin, J. K. Lee, Curr. Appl. Phys. **6**, 1030 (2006)

[12] R. Gopal, S. Kaur, Z. Ma, C. Chan, S. Ramakrishna, T. Matsuura, J. Membr. Sci. **281**, 581 (2006)

[13] E. Joussein, S. Petit, J. Churchman, B. Theng, D. Righi, B. Delvaux, Clay Miner. **40**, 383 (2005)

[14] C. C. Harvey, H. H. Murray, Clay Miner. Soc. Spec. Pub. **1**, 233 (1990)

[15] M. Liu, B. Guo, M. Du, F. Chen, D. Jia, Polymer **50**, 3022 (2009)

[16] Z. Jia, Y. Luo, S. Yang, B. Guo, M. Du, D. Jia, Chinese J. Polym. Sci. **27**, 857 (2009)

[17] R. Qi, R. Guo, M. Shen, X. Cao, L. Zhang, J. Xu, J. Yu, X. Shi, J. Mater. Chem. **20**, 10622 (2010)

[18] Y. M. Lvov, D. G. Shchukin, H. Möhwald, R. R. Price , ACS Nano **2**, 814 (2008)

[19] J. M. Deitzel, J. Kleinmeyer, D. Harris, N. C. B. Tan, Polymer **42**, 261 (2001)

[20] E. Zussman, A. L. Yarin, D. Weihs, Exp. Fluids **33**, 315 (2002)

[21] Y. Dong, D. Chaudhary, H. Haroosh, T. Bickford, J. Mater. Sci. **46**, 6148 (2011)

[22] A. H. Touny, J. G. Lawrence, A. D. Jones, S. B. Bhaduri, J. Mater. Res. **25**, 857 (2010)

[23] X. Jia, J. Zhang, W. Gao, H. Liang, H. Wang, J. Li, Mater. Lett. **63**, 658 (2009)

[24] Y. Dong, D. Bhattacharyya, Compos. Pt. A- Appl. Sci. Manuf. **39**, 1177 (2008)

[25] R. Khosrokhavar, G. Naderi, G. R. Bakhshandeh, M. H. R. Ghoreishy, Iran. Polym. J. **20**, 41 (2011)

[26] S. H. Park, *Robust design and analysis for quality engineering* (Chapman & Hall, London, 1996)

[27] S. Deng, J. Zhang, L. Ye, Compos. Sci. Technol. **69**, 2497 (2009)

[28] M. Murariu, A. L. Dechief, Y. Paint, S. Peeterbroeck, L. Bonnaud, P. Dubois, J. Polym. Environ. **20**, 932 (2012)

[29] K. Prashantha, B. Lecouvet, M. Sclavons, M. F. Lacrampe, P. Krawczak, J. Appli. Polym. Sci. **128**, 1895 (2012)

[30] W. S. Chow, S. K. Lok, J. Therm. Anal. Calorim. **95**, 627 (2009)

[31] J. T. Yoon, Y. G. Jeong, S. C. Lee, B. G. Min, Polym. Adv. Technol. **20**, 631 (2009)

[32] J. H. Lee, T. G. Park, H. S. Park, D. S. Lee, Y. K. Lee, S. C. Yoon, J. D. Nam, Biomaterials **24**, 2773 (2003)

[33] G. H. Lee, J. C. Song, K. B. Yoon, Macromol. Res. **18**, 571 (2010)

[34] A. Saraf, G. Lozier, A. Haesslein, F. K. Kasper, R. M. Raphael, L. S. Baggett, A. G. Mikos, Tissue Eng. Part C: Methods **15**, 333 (2009)

[35] Y. Dong, *Multi-scale effects on deformation mechanisms of polymer nanocomposite fibres: experimental characterisation and numerical study* (PhD thesis, The University of Auckland, New Zealand, 2008).

List of figures

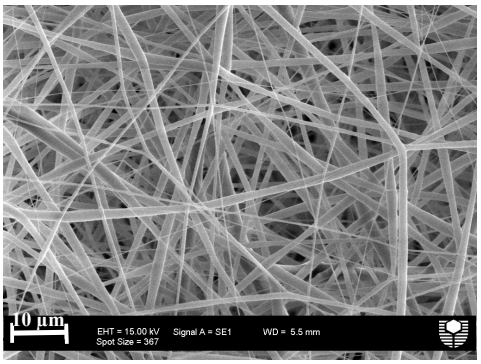

(a)

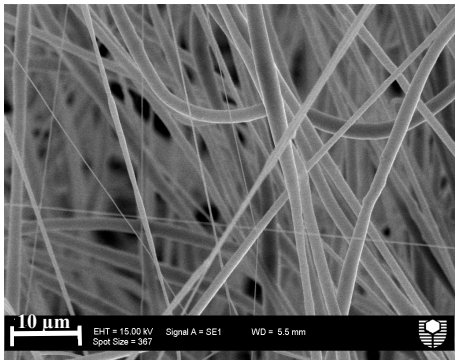

(b)

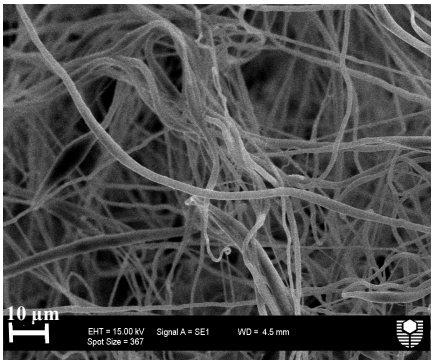

(c)

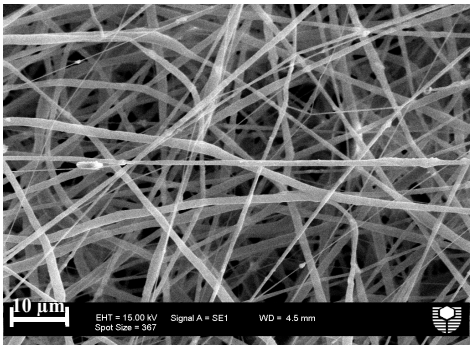

(d)

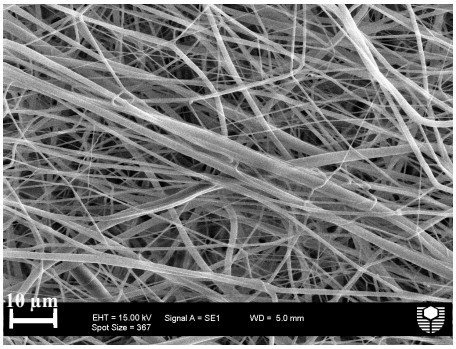

(e)

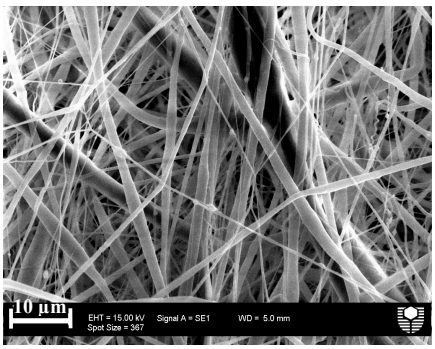

(f)

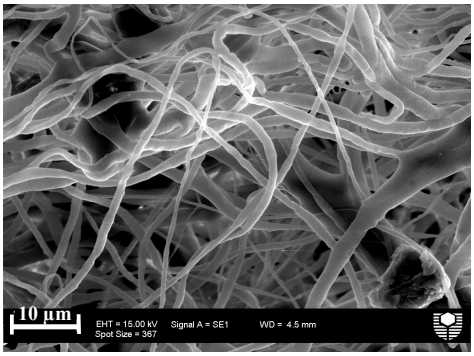

(g)

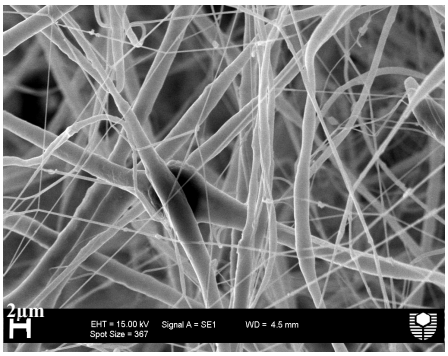

(h)

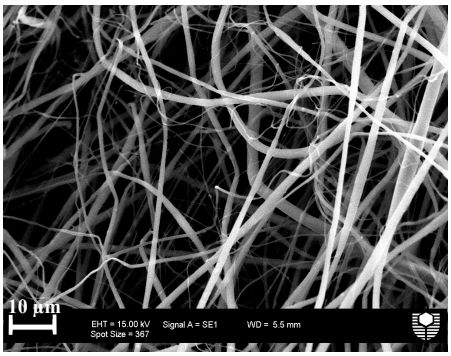

(i)

Fig. 1

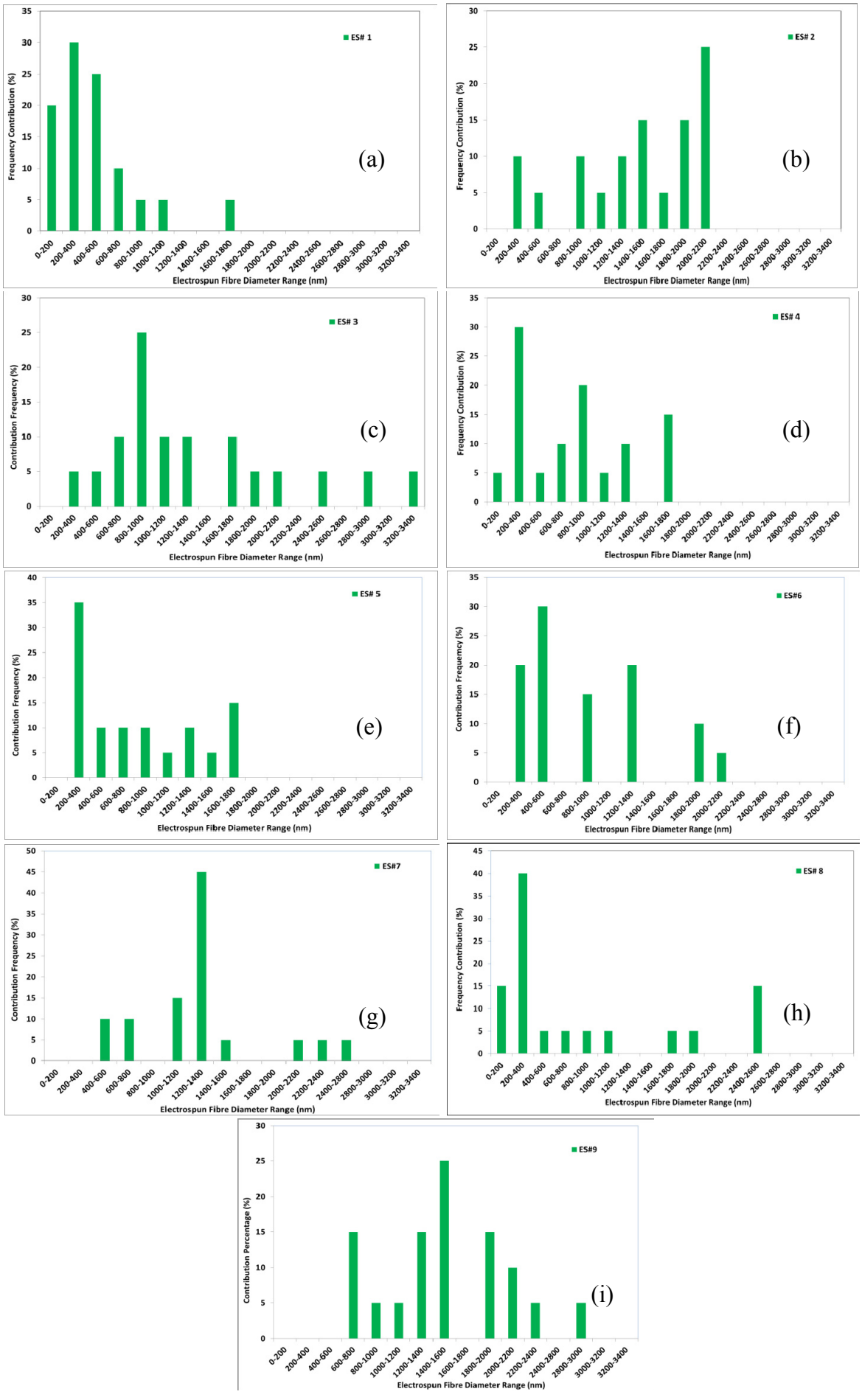
ES# 1
Frequency Contribution (%)
Electrospun Fibre Diameter Range (nm)
(a)
ES# 2
Frequency Contribution (%)
Electrospun Fibre Diameter Range (nm)
(b)
ES# 3
Contribution Frequency (%)
Electrospun Fibre Diameter Range (nm)
(c)
ES# 4
Frequency Contribution (%)
Electrospun Fibre Diameter Range (nm)
(d)
ES# 5
Contribution Frequency (%)
Electrospun Fibre Diameter Range (nm)
(e)
ES#6
Contribution Frequemcy (%)
Electrospun Fibre Diameter Range (nm)
(f)
ES#7
Contribution Frequency (%)
Electrospun Fibre Diameter Range (nm)
(g)
ES# 8
Frequency Contribution (%)
Electrospun Fibre Diameter Range (nm)
(h)
ES#9
Contribution Percentage (%)
Electrospun Fibre Diameter Range (nm)
(i)

Fig. 2

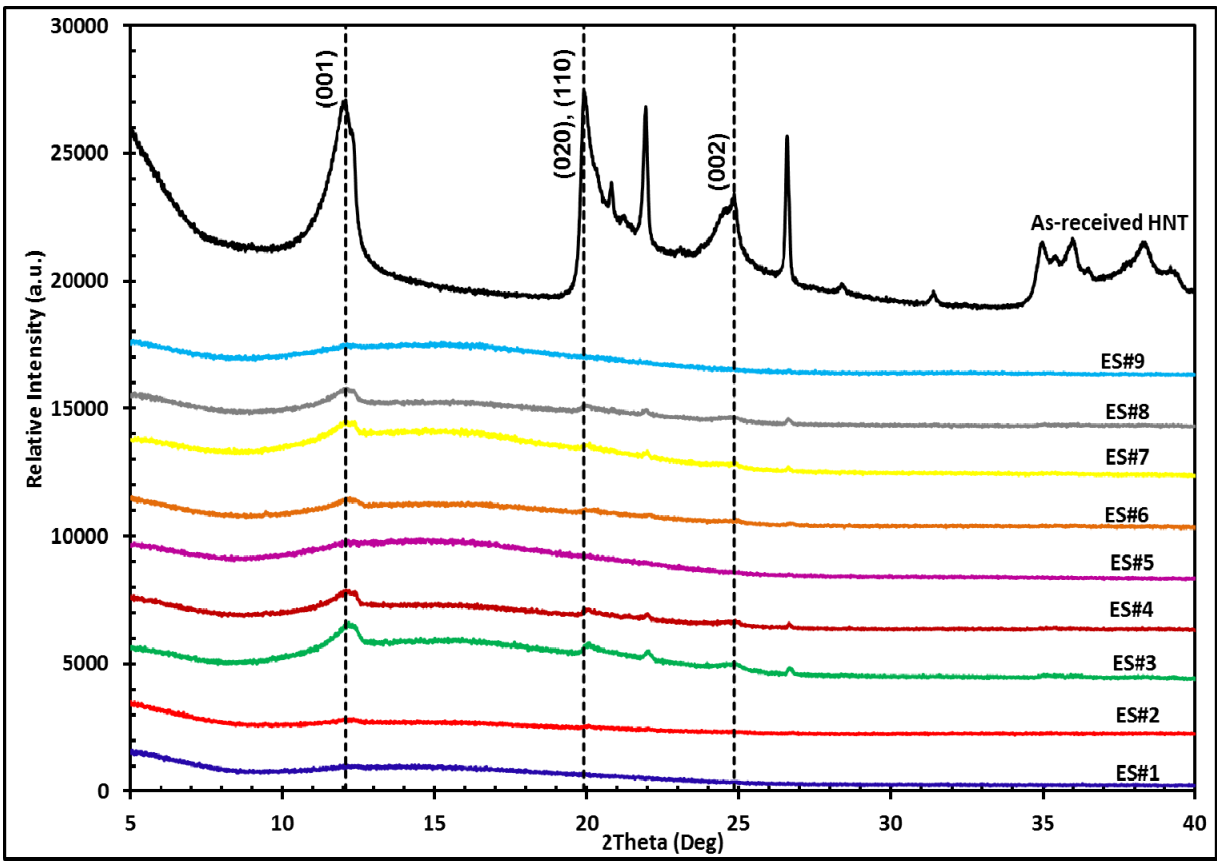
30000
25000
20000
15000
10000
5000
0
Relative Intensity (a.u.)
5
10
15
20
25
30
35
40
2Theta (Deg)
(001)
(020), (110)
(002)
As-received HNT
ES#9
ES#8
ES#7
ES#6
ES#5
ES#4
ES#3
ES#2
ES#1

Fig. 3

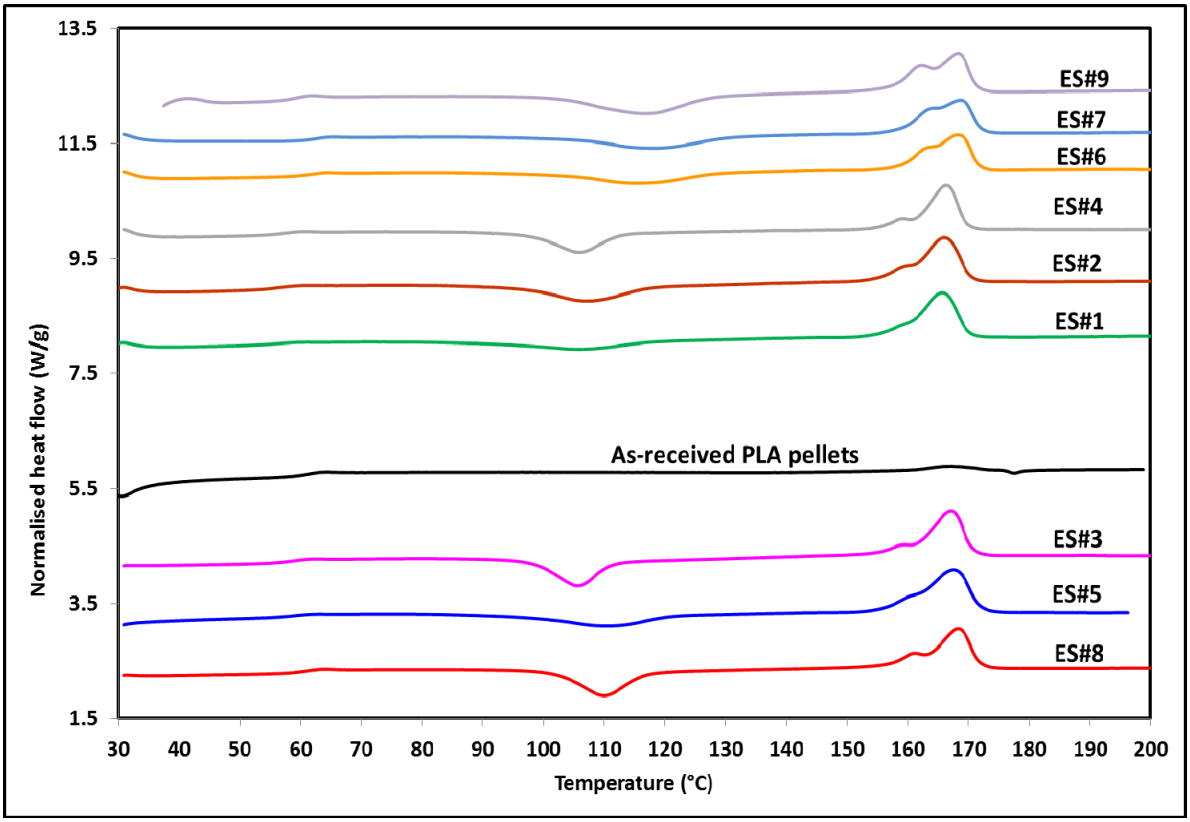
13.5
11.5
9.5
7.5
5.5
3.5
1.5
Normalised heat flow (W/g)
30
40
50
60
70
80
90
100
110
120
130
140
150
160
170
180
190
200
Temperature (°C)
ES#9
ES#7
ES#6
ES#4
ES#2
ES#1
As-received PLA pellets
ES#3
ES#5
ES#8

Fig. 4

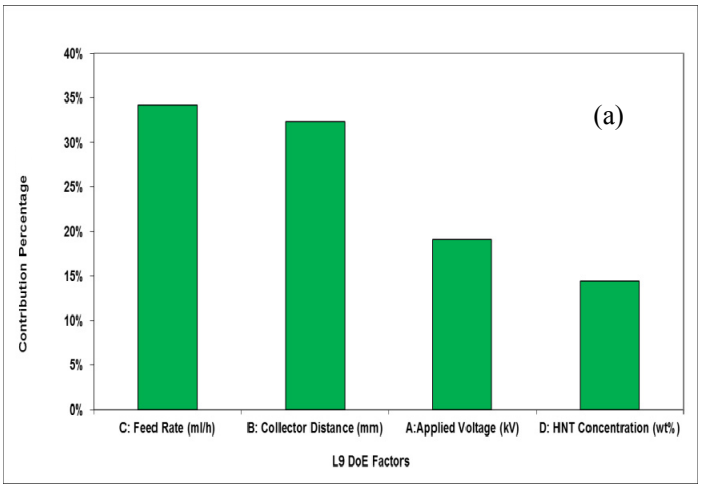
(a)
Contribution Percentage
40%
35%
30%
25%
20%
15%
10%
5%
0%
C: Feed Rate (ml/h)
B: Collector Distance (mm)
A:Applied Voltage (kV)
D: HNT Concentration (wt%)
L9 DoE Factors

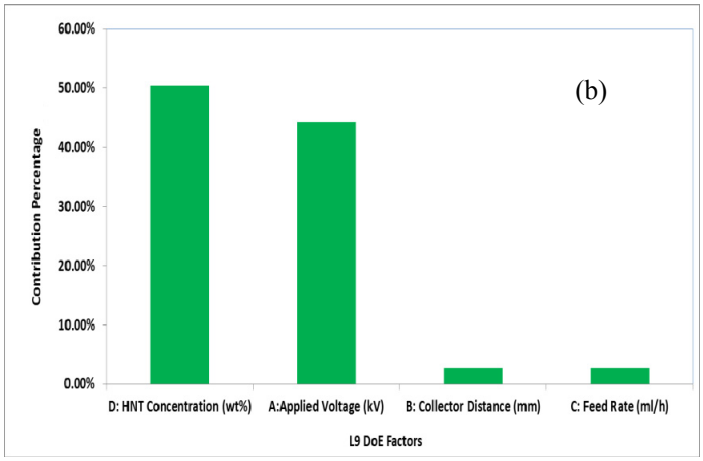
(b)
Contribution Percentage
60.00%
50.00%
40.00%
30.00%
20.00%
10.00%
0.00%
D: HNT Concentration (wt%)
A:Applied Voltage (kV)
B: Collector Distance (mm)
C: Feed Rate (ml/h)
L9 DoE Factors

Fig. 5

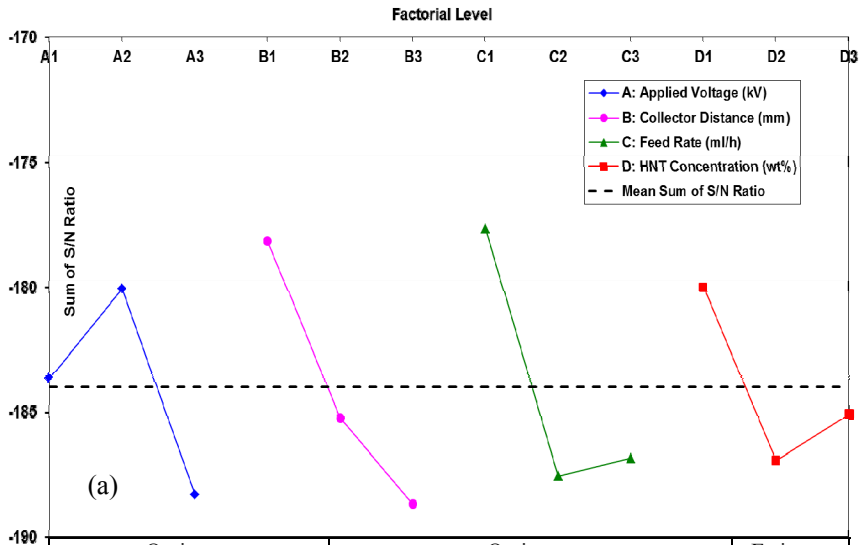

Optimum Factorial Level Combination	Optimum Processing Condition	Estimate of Error Variance
$A_2B_1C_1D_1$	21 kV voltage/90 mm collector distance/ 1ml/h feed rate/1.5 wt% HNTs	8.543

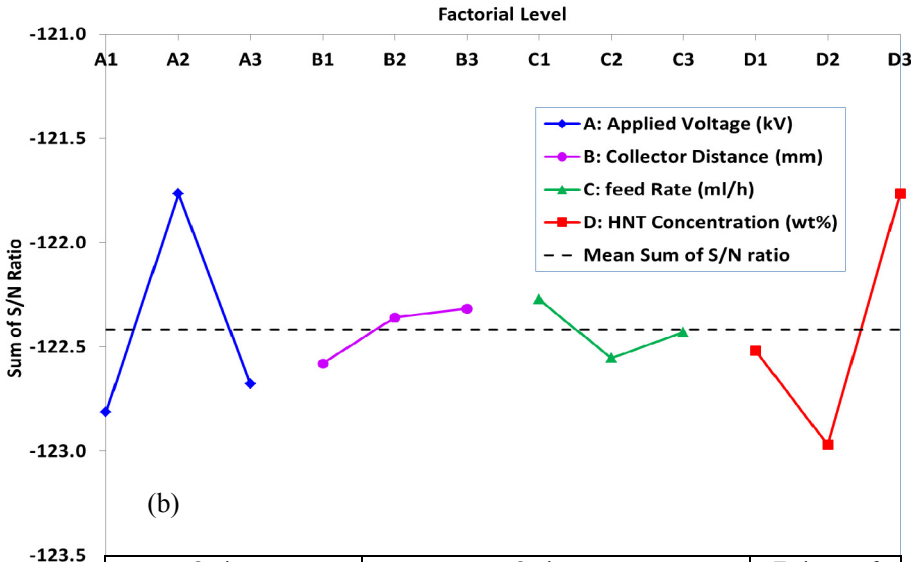

Optimum Factorial Level Combination	Optimum Processing Condition	Estimate of Error Variance
$A_2B_3C_1D_3$	21 kV voltage/150 mm collector distance/ 1ml/h feed rate/10 wt% HNTs	0.013

Fig. 6

Table 1 Four factors and three levels selected in L_9 DoE array

Factor	Level		
	1	2	3
A: Applied voltage (kV)	16	21	27
B: Collector distance (mm)	90	120	150
C: Feed rate (ml/h)	1	2	4
D: HNT concentration (wt%)	1.5	5	10

Table 2 L_9 DoE layout for electrospinning process

Experiment number	Factors			
	A: Applied voltage (kV)	B: Collector distance (mm)	C: Feed rate (ml/h)	D: HNT concentration (wt %)
ES# 1	16	90	1	1.5
ES# 2	16	120	2	5
ES# 3	16	150	4	10
ES# 4	21	90	2	10
ES# 5	21	120	4	1.5
ES# 6	21	150	1	5
ES# 7	27	90	4	5
ES# 8	27	120	1	10
ES# 9	27	150	2	1.5

Table 3 Average fibre diameter d_{aver} and its associated typical frequency contribution (FC) of PLA/HNT composite fibres in DoE study

Experiment number	Average fibre diameter d_{aver} (nm)	Standard deviation (nm)	Frequency contribution (FC) (%)		
			$d_{aver} \leq 1\mu m$	$d_{aver} \leq 600$ nm	$d_{aver} \leq 400$ nm
ES#1	498	374	90	75	50
ES#2	1424	615	25	15	10
ES#3	1393	802	45	10	5
ES#4	814	516	70	40	35
ES#5	854	546	65	45	35
ES#6	875	598	65	50	20
ES#7	1273	519	20	10	0
ES#8	833	853	70	60	55
ES#9	1518	569	20	0	0

Table 4 XRD pattern characteristics of as-received HNTs and PLA/HNT composite fibres in DoE study

Reflection plane	(001)		(020), (110)		(002)	
XRD sample	2θ	d (nm)	2θ	d (nm)	2θ	d (nm)
As-received HNTs	12.09	0.732	19.90	0.446	24.85	0.358
ES#1	12.25	0.722				
ES#2	12.20	0.725	20.05	0.443		
ES#3	12.19	0.726	20.04	0.443	24.85	0.358
ES#4	12.10	0.731	19.95	0.445	24.89	0.358
ES#5	12.17	0.727				
ES#6	12.23	0.724	19.95	0.445	24.91	0.357
ES#7	12.09	0.732	20.09	0.442	24.84	0.358
ES#8	12.11	0.730	19.93	0.445	24.72	0.360
ES#9	12.14	0.729				

Table 5 DSC characteristic parameters for as-received PLA pellets and PLA/HNT composite fibres (ES#1-ES#9)

DSC sample	T_g (°C)	T_c (°C)	T_{m1} (°C)	T_{m2} (°C)
As-received PLA pellets	61.5 (±0.7)	140 (± 0)		167.6 (±0.8)
ES#1	60.5 (±3.8)	111.8 (±5.0)		167.1 (±1.1)
ES#2	60.7 (±3.8)	114.0 (±5.9)	161.9 (±2.2)	167.6 (±1.3)
ES#3	59.4 (±0.9)	108.3 (±2.2)	159.5 (±0.8)	167.6 (±0.4)
ES#4	57.2 (±0.2)	105.6 (±0.0)	158.6 (±0.1)	166.3 (±0.0)
ES#5	58.9 (±0.4)	107.2 (±3.0)		166.1 (±1.3)
ES#6	59.3 (±2.7)	108.1 (±7.2)	158.5 (±4.0)	166.6 (±1.6)
ES#7	61.3 (±1.1)	113.9 (±4.1)	161.5 (±1.8)	167.7 (±0.8)
ES#8	59.1 (±1.5)	107.2 (±2.8)	159.1 (±1.4)	166.5 (±1.7)
ES#9	59.7 (±0.6)	111.3 (±4.9)	161.3 (±0.6)	167.1 (±1.1)

The values in the parentheses are standard deviations calculated from DSC measurements.